THE ASTROPHYSICAL JOURNAL, 469:662–675, 1996 October 1

ASCA OBSERVATIONS OF STARBURSTING DWARF GALAXIES: THE CASE OF NGC 1569

ROBERTO DELLA CECA,[1] RICHARD E. GRIFFITHS, AND TIMOTHY M. HECKMAN
Department of Physics and Astronomy, The Johns Hopkins University, Charles and 34th Streets, Baltimore, MD 21218

AND

JOHN W. MACKENTY
Space Telescope Science Institute, 3700 San Martin Drive, Baltimore, MD 21218
Received 1995 December 14; accepted 1996 April 15

ABSTRACT

We present *ASCA* observations of the nearby star-forming dwarf galaxy NGC 1569. Combining the *ASCA* data with archival *ROSAT* PSPC and HRI data, optical broad and narrow Hα images, and new infrared *K*-band images, we have investigated, in greater detail than previously possible, the X-ray properties of this prototype dwarf starburst.

The principal results of this investigation are as follows:

1. The *ASCA* SIS broad-band (0.5–6 keV) X-ray spectrum reveals the presence of at least two spectral components. The soft component is best described by a thermal model with a temperature of ∼0.64–0.8 keV, while the hard component can be described by a thermal model with a temperature of ∼3.7 keV or by a power law with photon index of ∼2.1. The total unabsorbed X-ray luminosity is $\sim 3.1 \times 10^{38}$ ergs s^{-1} (0.5–2.0 keV) and $\sim 1.3 \times 10^{38}$ ergs s^{-1} (2–10 keV). The soft thermal component provides ∼60% of the total luminosity in the (0.5–2.0) keV energy band but less than ∼10% of the total luminosity in the 2–10 keV energy band.

2. The *ROSAT* PSPC image of NGC 1569 shows that the soft ($E < 2$ keV) X-ray emission is clearly extended, is morphologically associated with the system of Hα filaments (in which NGC 1569 is immersed), and seems to extend preferentially along the optical minor axis of the galaxy. In the azimuthally averaged and background-corrected radial profile, the soft X-ray emission (from the *ROSAT* PSPC) can be detected out to a radius of ∼1.9 (≃1.2 kpc); the half-light radius is ∼28″ (≃0.29 kpc). The soft X-ray emission profile (from the *ASCA* SIS) can be described by a simple model consisting of a pointlike X-ray source along with diffuse X-ray emission described by a bidimensional Gaussian distribution with $\sigma \sim 30''$ (≃0.31 kpc). About 40% of the soft X-ray emission derives from the pointlike source and the remainder from the diffuse emission. The hard ($E > 2$ keV) X-ray emission is consistent with a pointlike source (the central starburst) at the spatial resolution of the *ASCA* XRT + SIS system.

3. The *ROSAT* HRI image resolves the central starburst into a group of at least four bright knots of X-ray emission. Almost all the flux in the hard spectral component could be associated with the two brightest knots of X-ray emission. If this is the case, the spectral shape that we observe for the hard spectral component suggests an origin of the X-ray emission in young supernova remnants or in low-mass X-ray binaries.

The new *ASCA* data provide crucial support for the idea that starbursts can drive gas out of dwarf galaxies. First, the data establish that the diffuse X-ray emission in NGC 1569 is produced by hot gas. Second, they show that the temperature of this gas far exceeds the depth of the galaxy's shallow potential well.

The data also suggest that a population of galaxies like NGC 1569 would have X-ray spectra that are too soft to contribute significantly to the hard (>2 keV) cosmic X-ray background. These objects contribute in a major way to the soft X-ray background only.

Subject headings: galaxies: individual (NGC 1569) — galaxies: starburst — X-rays: galaxies

1. INTRODUCTION

Dwarf galaxies are the most numerous galaxies in the local and moderate-redshift universe. According to the currently popular "bottom-up" cosmological scenarios, they should represent the sites of the earliest star formation and the basic building blocks for larger galaxies (see Blumenthal et al. 1984 and references therein). This scenario is now supported by the deepest *Hubble Space Telescope* (*HST*) survey data, in which there is increasing evidence for irregular type starburst activity with increasing survey depth (Driver, Windhorst, & Griffiths 1995a; Driver et al. 1995b; Glazebrook et al. 1995; Cowie, Hu, & Songaila 1995; Abraham et al. 1996).

Optical imaging and spectroscopy of some of the nearby dwarf star-forming galaxies has led to the discovery of kiloparsec-scale expanding "bubbles" of ionized gas, which are presumably inflated by the supernovae and stellar winds in the central starburst (Meurer et al. 1992; Marlowe et al. 1995; Martin 1996).

Theoretical work (see, e.g., Babul & Ferguson 1996) has shown that such a wind could have a particularly devastating impact on the structure and evolution of dwarf galaxies, and, in particular, any actively star-forming dwarf galaxy

[1] Present address: Osservatorio Astronomico di Brera, via Brera 28, 20121, Milano, Italy; rdc@brera.mi.astro.it.

should be suffering substantial mass loss as its interstellar medium (ISM) is heated and ejected. The process of supernova-driven galactic winds can naturally explain the low metal abundances and low surface brightnesses of dwarf galaxies (see Dekel & Silk 1986; Yoshii & Arimoto 1987) and the transformation of one type of dwarf galaxy into another (see Ferguson & Binggeli 1994) and may be responsible for a substantial fraction of the metal abundances of the intergalactic medium (Lynden-Bell 1992).

The most direct probe of the hot wind material is provided by X-ray data. While the optical emission lines arise in ambient gas that is shocked by the wind, the X-rays should come (at least in part) directly from the wind fluid itself. X-ray data therefore provide a strong constraint on the overall hypothesized picture.

Dwarf star-forming galaxies have been also proposed as substantial contributors to the cosmic X-ray background (Griffiths & Padovani 1990). Recent *ROSAT* results (Griffiths et al. 1996) show that up to 40% of the soft (0.5–2 keV) X-ray background could be due to luminous starburst galaxies, but their contribution at higher energies is not well constrained because the spectral properties of this class of objects are not well known at $E > 2$ keV. This class of objects could produce a substantial fraction of the 2–10 keV X-ray background, especially if their hard X-ray emission is dominated by massive X-ray binaries in regions of low metallicity (like the massive X-ray binaries in the Magellanic Clouds).

The importance of dwarf galaxies toward our overall understanding of the formation and evolution of galaxies is thus clear, as is their significance in many areas of current observational cosmology (see reviews by Hunter & Gallagher 1989; Binggelli 1994; Gallagher & Wyse 1994; Ferguson & Binggeli 1994). Studies of local examples are thus extremely important. Prompted by these considerations we have initiated a program of *ASCA* (*Advanced Satellite for Cosmology and Astrophysics*) observations of nearby and well-known star-forming dwarf galaxies with the following specific aims:

1. To verify spectroscopically the presence of multiple components in the X-ray emission, to measure their respective luminosities, and to evaluate their proportional contribution in the soft ($E < 2$ keV) and hard ($E > 2$ keV) energy band.
2. Specifically, to investigate the presence of a diffuse soft X-ray component, to evaluate its global extent, and to compare this extent with the optical and radio size scales.
3. To compare the X-ray spectrum of the hard component with that of the cosmic X-ray background.

In this paper, we present *ASCA* results on NGC 1569 (also known as Arp 210 and VII Zw 16), the nearest and best studied example of a starbursting dwarf galaxy. We have compared the *ASCA* data with archival *ROSAT* Position Sensitive Proportional Counter (PSPC) and High Resolution Imager (HRI) data, optical broad-band and narrow-band Hα images, and new infrared *K*-band images; we have thus been able to investigate, in greater detail than previously possible, the overall properties of this prototype object.

In § 2 we discuss the overall properties of NGC 1569 based on previous observations. The *ASCA* data, the archival *ROSAT* HRI and PSPC data, and the new *K*-band infrared observations are presented and discussed in § 3. In § 4 we compare the X-ray images obtained from the *ROSAT* HRI and PSPC with the optical (narrow- and broad-band) and the infrared images. In this section we also investigate the soft and hard X-ray radial profile obtained from the *ASCA* SIS data. The spectral analysis of the *ASCA* data and the *ROSAT* PSPC data is presented in § 5. Section 6 contains a discussion of the results in the context of models for starbursts and starburst-driven outflows and a discussion of the relevance of these observations to the contribution of dwarf star-forming galaxies to the cosmic X-ray background. Finally, in § 7 a summary and conclusions are presented.

2. NGC 1569: OVERALL PROPERTIES AND PREVIOUS OBSERVATIONS

NGC 1569 is a Magellanic-type irregular galaxy located at a distance of 2.2 ± 0.6 Mpc (Israel 1988). At this distance, $1' \simeq 0.63$ kpc. Optical continuum images show NGC 1569 to be a rather flat system ($a/b \sim 2$), with the major axis at a position angle of $\sim 120°$ and an optical size (at the limiting surface brightness of 25 *B* mag arcsec^{-2}, after correction for Galactic extinction) of about 2.3×1.15 kpc (adapted from de Vaucouleurs et al. 1991). At the assumed distance, NGC 1569 has an absolute blue magnitude of $M_B = -17$ ($L_B = 10^9\ L_\odot$).

The total dynamical mass within a radius of 1.3 kpc is only $M_T \simeq 3.4 \times 10^8\ M_\odot$ (Reakes 1980), and almost half of M_T resides in neutral atomic gas (H I, He I) (Israel 1988). The H I distribution (Israel & van Driel 1990) is described by a bright ridge with three maxima surrounded by more extended diffuse emission and by a 190 pc hole centered on one of the two superstar clusters belonging to NGC 1569 (see O'Connell, Gallagher, & Hunter 1994). The H I diffuse emission extends well beyond the optical size of the galaxy; its dimensions, at an H I column density of 1.8×10^{20} cm^{-2}, are about $7' \times 3'.5$ ($\simeq 4.4 \times 2.2$ kpc).

NGC 1569 has an extensive literature (see Israel 1988; Waller 1991), and its overall properties have been recently summarized and discussed by Heckman et al. (1995, hereafter H95), who also present *ROSAT* HRI observations and new long-slit optical spectra.

NGC 1569 is characterized by extremely blue optical colors [$(U-B)_o = -0.62$, $(B-V)_o = 0.23$; Israel 1988], large Hα luminosity ($L_{H\alpha} \simeq 5 \times 10^{40}$ ergs s^{-1}; Waller 1991 and references therein), and strong, warm IR emission ($L_{1-500\ \mu m} \simeq 7 \times 10^8\ L_\odot$, $S_{60\ \mu m} \sim S_{100\ \mu m}$;Israel 1988). NGC 1569 also has a nonthermal bright radio halo (Israel & de Bruyn 1988), which has an extent of ~ 2.2 kpc in diameter. This halo is thought to be produced by synchrotron emission from relativistic electrons flowing out from the central starburst.

Deep Hα images (Hodge 1974; Waller 1991; Hunter, Hawley, & Gallagher 1993) indicate that NGC 1569 is immersed in a bright and morphologically complex system of emission-line filaments and loops. These features extend to several kiloparsecs and are preferentially oriented along the minor axis of the galaxy. Several holes in the ionized gas have been noted by Hunter et al. (1993). The kinematics of this gas have been studied recently by Tomita, Ohta, & Saito (1994) and H95. H95 found that the Hα emission comprises two kinematically distinct components. The first component, which produces $\sim 75\%$ of the total Hα emission, is relatively quiescent ($v \leq v_{sys} \pm 30$ km s^{-1}) and is located within the central kpc of the galaxy; this component

probably corresponds to the gas in the starbursting disk. The second component is a more complex system: it extends over 2 kpc in size with radial velocities up to ± 200 km s^{-1} relative to v_{sys}. This latter component appears to define expanding hollow structures consisting of several kiloparsec-scale "superbubbles" (first described by de Vaucouleurs, de Vaucouleurs, & Pence 1974).

3. THE DATA

3.1. *ASCA Observations and Data Preparation*

NGC 1569 was observed by *ASCA* (Tanaka, Inoue, & Holt 1994) from 1994 October 5 through 1994 October 7. At the focal plane of its four X-ray telescopes (XRT), there are two Solid-State Imaging Spectrometers (hereafter SIS0 and SIS1 or in general SIS) and two Gas Imaging Spectrometers (hereafter GIS2 and GIS3 or in general GIS)

The point-spread function (PSF) of the *ASCA* XRT is characterized, to a first approximation, by a relatively sharp core (FWHM $\sim 50''$) and broad wings of half-power radius $1'.5$. Furthermore, unlike the SIS (that can be considered as a perfect imager) the GIS has its own PSF which is comparable with the XRT PSF. Consequently, the convolved PSF of the XRT + GIS system is much broader than that of the XRT alone. *ROSAT* PSPC and HRI observations of the NGC 1569 field reveal the presence of a bright X-ray source located about $3'$ to the east-southeast of NGC 1569. This X-ray source, identified with a star by H95, has a *ROSAT* PSPC broad-band (0.1–2.4 keV) count rate that is about 65% of the PSPC count rate derived from NGC 1569 itself (see § 4.2 and H95). Because of the broad XRT + GIS PSF, this source is heavily confused with NGC 1569 in the GIS data set. Therefore, as far as our *ASCA* results are concerned, we will concentrate on the SIS data.

Data preparation and analysis have been done using version 1.2 of the XSELECT software package (Ingham 1994) and version 3.2 of FTOOLS (Blackburn et al. 1995). Good time intervals were selected by applying the data selection criteria shown in Table 1. From an inspection of the light curve, we were also able to reject periods of high count rate due to background variations. The total effective exposure time was 78,065 s for SIS0 and 76,900 s for SIS1.

During these *ASCA* observations, the SIS was operating in 1 CCD Bright and Faint modes. Faint data were converted into Bright mode. Hot and flickering pixels were removed using SISCLEAN (inside the FTOOLS software package) and by applying the parameters reported in Table 1.

Spectral analysis has been performed using version 8.50 of the XSPEC software package (Arnaud 1996). The counts from the source and from the background regions were extracted in the Pulse Invariant (PI) energy channels, which have been corrected for spatial and temporal variations of the detector gain. We used the detector Redistribution Matrix Files (RMF) s0c1g0234p40e1_512v0_8i.rmf and s1c3g0234p40e1_512v0_8i.rmf for SIS0 and SIS1, respectively. The Ancillary Response Files (ARF) were created using version 2.3 of the task *ASCA*ARF (inside the FTOOLS software package) at the location of NGC 1569 in the detectors (see George et al. 1992 for the definition of the RMF and ARF calibration files).

3.2. *ROSAT HRI and PSPC Observations and Data Preparation*

NGC 1569 was observed in pointed mode with the *ROSAT* HRI (David et al. 1993) for a total of 11,268 s on 1992 March 14–15 (ROS:rh600157; PI:T.Heckman). This observation has been extensively discussed by H95. The principal results obtained by these authors can be summarized as follows: at least half of the $\sim$0.7–1.7 keV X-ray emission arises in a diffuse, nonspherical halo that is some $3'.8 \times 2'.3$ ($\simeq 2.4 \times 1.5$ kpc) in size and that is morphologically associated with the system of Hα filaments. In particular, it is worth noting that this diffuse X-ray emission, which has L_X (0.1–2.4 keV) $\sim 3 \times 10^{38}$ ergs s^{-1} (assuming a conversion factor appropriate for a Raymond-Smith thermal model with $kT \simeq 0.8$ keV), extends outward along or near the optical minor axis of the galaxy. The remainder of the X-ray emission arises in a knotty region several hundred parsecs in size positionally coincident with the central starburst. For the purpose of this paper, we have produced a high-resolution HRI image in the following way: we have first created an X-ray image with a pixel size of $1''.5$ and then smoothed this image with a Gaussian having a FWHM $\sim 3''.5$. The HRI image created in this way preserves the intrinsic FWHM of the on-axis HRI PSF ($\sim 5''$).

NGC 1569 was observed with the *ROSAT* PSPC (Pfefferman et al. 1987) on 1993 February 16–23 (ROS:rp600138n00; PI:H.Thronson) and on 1993 August 20 (ROS:rp600138a01; PI:H.Thronson). Both these observations were made in pointed mode with the object at the center of the PSPC (detector B) field. We have combined these two data sets; the total observing time for the combination is 7765 s. In order to preserve the intrinsic FWHM of the on-axis PSPC PSF, we have first produced a broad-band (0.1–2.4 keV) image with a pixel size of $4''$ and then smoothed this image with a Gaussian of FWHM $\sim 19''$. We have also slightly corrected the nominal position of the field center of the *ROSAT* PSPC observation by using six bright pointlike X-ray sources in the PSPC image and the corresponding probable optical counterparts visible on the Palomar Observatory Sky Survey (POSS) plates. The positional accuracy of the corrected image is better than $10''$.

TABLE 1

SELECTION CRITERIA AND CLEANING PARAMETERS FOR *ASCA* SIS

Criterion/Parameter	Value
Data Selection Criteria	
ONTIME	>100
NEVENTS	>0
SAA	0
T_SAA	<0 or >60
FOV	0
ELV_MIN	>5
BR_EARTH	>25 (SIS0); >20 (SIS1)
T_DY_NT	<0 or >100
COR_MIN	>6
S0_PIXL1 (SIS0)	>0 and <400
S1_PIXL3 (SIS1)	>0 and <400
SISCLEAN Parameters	
clean	2
cellsize	5
log_prob	−5.24
bkg_thr	3
clean_phalow	0
clean_phahi	4095

NOTE.—For a detailed description of the parameters used, the reader is referred to Day et al. 1995.

Because the exposure map is constant at better than 1% inside the central 5′ of the *ROSAT* PSPC field, we have not applied any correction for it.

It is worth noting that because of the high Galactic column density along the line of sight to NGC 1569 ($N_H = 2.1 \times 10^{21}$ cm^{-2}; see H95 and references therein), our data provide very little direct information on this object for $E \lesssim 0.6$–0.7 keV.

For the analysis of the *ROSAT* PSPC and HRI data, we have used the IRAF/PROS software package and the XSPEC software package. For the spectral analysis of the *ROSAT* PSPC data (see § 5), we have used the detector response matrix pspcb_93jan12.rsp.

3.3. *Infrared Observations*

NGC 1569 was observed with Kitt Peak National Observatory's 1.3 m telescope and the Simultaneous Quad-Color Infrared Imaging Device (SQIID). This instrument has four 256 × 256 Hughes PtSi arrays mounted behind reimaging optics that simultaneously view the same region of the sky in the *J*, *H*, *K*, and *L* passbands (Ellis et al. 1993). The plate scale was 1.″36 pixel^{-1}. These observations were obtained on 1990 September 3 UT during an early engineering run with SQIID with engineering grade detectors and under rather unfavorable atmospheric conditions (high humidity and scattered clouds). Five exposures of 180 s duration each with 50″–75″ motions between each exposure were acquired. The airmass ranged from 1.60 to 1.66. These frames were dark-subtracted, flat-fielded with the median of a large number of sky images, registered, and averaged.

4. SPATIAL ANALYSIS

4.1. *ROSAT HRI*

In Figure 1 we show a contour map representation of the smoothed *ROSAT* HRI image overlaid on the infrared *K*-band image. We have determined the astrometry of the latter using about 10 objects and their counterparts on the POSS plate. To correct the nominal position of the field center of the *ROSAT* HRI pointing position was more difficult. This observation contains only the star located about 3′ to the east-southeast of NGC 1569 (see § 4.2 and Fig. 3) for which the X-ray centroid can be determined with accuracy, and, therefore, the optical counterpart can be unambiguously identified on the POSS plate. We have used this star to correct the astrometry of the *ROSAT* HRI image: the applied correction amounts to 3.″8 in right ascension and − 1.″2 in declination. The displayed X-ray contour levels correspond to 2.5 σ, 3 σ, 5 σ, 7 σ, 10 σ, 20 σ, 30 σ, and 50 σ above the background. We have determined the background level of the original 1.″5 × 1.″5 HRI image by calculating the mean count rate in six source-free regions of the sky around NGC 1569. The results for these regions were very similar; the mean value of the background was 0.03 counts pixel^{-1} (=0.0133 counts arcsec^{-2}) with a corre-

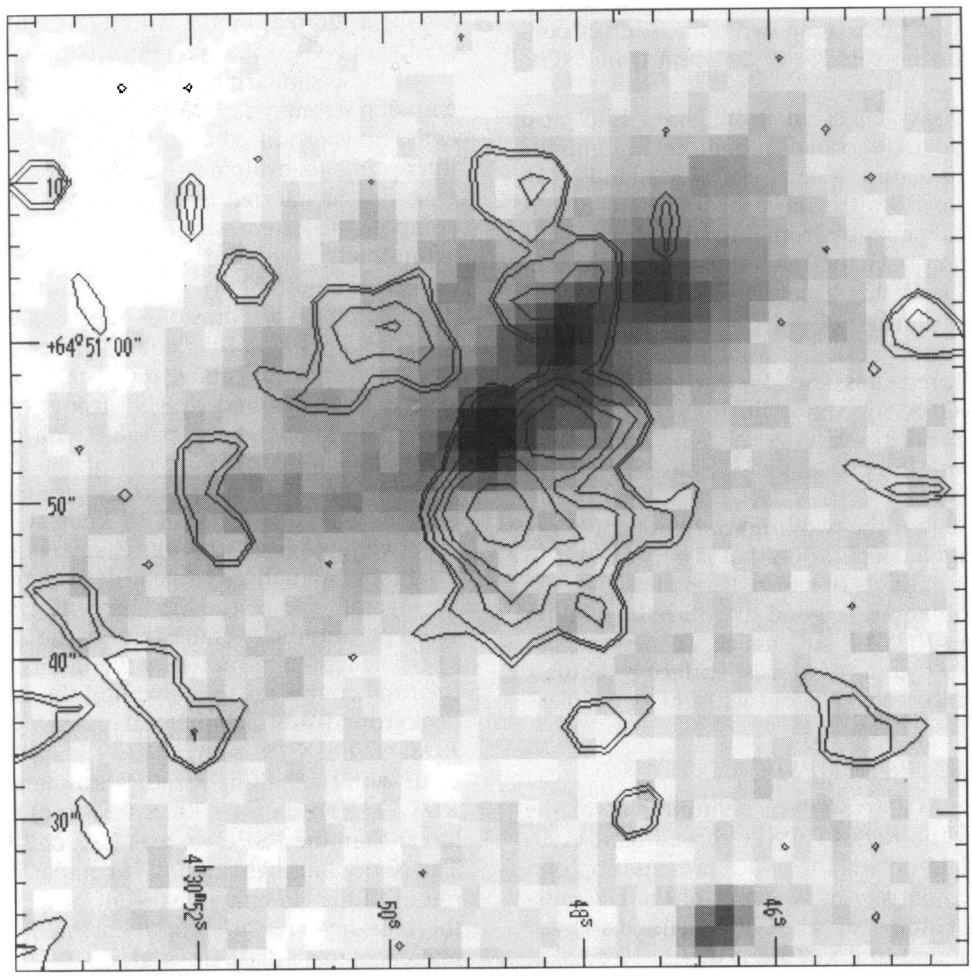

FIG. 1.—Gray-scale infrared *K*-band image with overlaid X-ray emission contour obtained from the smoothed *ROSAT* HRI image of NGC 1569. The smoothed *ROSAT* HRI image has been created from the raw HRI data first by blocking into 1.″5 pixels, then by smoothing with a Gaussian having a FWHM ~ 3.″5. The displayed X-ray contour levels correspond to 2.5 σ, 3 σ, 5 σ, 7 σ, 10 σ, 20 σ, 30 σ, and 50 σ above the background (see § 4.1 for details).

sponding standard deviation (σ) of 0.173 counts pixel^{-1}. The standard deviation of the smoothed image (σ_{smo}) was computed using the formula (Rosati 1995)

$$\sigma_{smo} = \sigma \frac{1}{2\pi^{0.5}\sigma_G},$$

where σ_G is the standard deviation of the Gaussian smoothing function (=1 pixel for this particular case). We detect a total of 163 $\pm$ 29 net counts (hereafter for "net counts" we mean the background-subtracted counts) within a radius of 2′ from the peak of the X-ray emission, which implies a count rate of 0.015 $\pm$ 0.003 counts s^{-1} for the 11,268 s of observation. All these numbers are in agreement with the analysis previously reported in H95.

As can be seen in Figure 1, the central soft ($E \lesssim 2$ keV) X-ray emission from NGC 1569 is resolved into a group of at least four bright knots of X-ray emission. The X-ray fluxes and luminosities of the two brightest blobs have been determined by H95 assuming a count-to-flux conversion factor appropriate for thermal emission from warm gas with $kT = 0.8$ keV (see Table 2 of H95). The lower blob has an unabsorbed (0.1–2.4 keV) X-ray flux of $1.6 \pm 0.4 \times 10^{-13}$ ergs cm^{-2} s^{-1} with a corresponding luminosity of about 1×10^{38} ergs s^{-1}, while for the upper blob, the flux and luminosity are $0.8 \pm 0.3 \times 10^{-14}$ ergs cm^{-2} s^{-1} and 5×10^{37} ergs s^{-1}, respectively. If a count-to-flux conversion factor appropriate for thermal emission from hot gas with $kT = 5$ keV is adopted, all the above quantities increase by a factor 1.4. As noted in H95, these two point sources contribute about 30% of the soft X-ray emission from NGC 1569.

The central soft X-ray emission from NGC 1569 also shows a lumpy ridge that extends about 50″ along the galaxy major axis (this feature is more clearly seen in Fig. 1*b* of H95). According to H95, the more likely origin of this lumpy ridge is thermal emission from diffuse hot gas inside the body of the galaxy. On the assumption of a thermal model with $kT \sim 0.8$ keV, this structure has an unabsorbed (0.1–2.4) keV flux (luminosity) of $\sim 1.7 \times 10^{-13}$ ergs cm^{-2} s^{-1} ($L_X \sim 1 \times 10^{38}$ ergs s^{-1}).

Three knots of infrared emission are clearly visible in the *K*-band image of NGC 1569 shown in Figure 1; the two brightest knots are positionally consistent, within the astrometric errors, with the two super–star clusters studied by O'Connell et al. (1994).

It is very suggestive that the two brightest knots of X-ray emission show an angular separation that is very similar to that of the two brightest knots of infrared emission. Because of the difficulty in obtaining a good astrometric solution (better than 5″) for this *ROSAT* HRI image, we are forced to speculate that the two regions of highest surface brightness in soft X-rays could also be coincident with the two super–star clusters.

4.2. *ROSAT PSPC*

In Figure 2 (Plate 41), we show a contour plot of the X-ray emission from the *ROSAT* PSPC broad-band (0.1–2.4 keV) image overlaid on a color plot representation of a continuum-subtracted narrow-band image of the Hα emission (published in Hunter et al. 1993). The displayed contour levels correspond to 2.5 σ, 3 σ, 5 σ, 7 σ, 10 σ, 20 σ, 30 σ, and 50 σ above the background (0.0188 counts pixel^{-1} = 1.2×10^{-3} counts arcsec^{-2}), determined in a similar way as for the *ROSAT* HRI image. We detect a total of 300 $\pm$ 20 net counts within a radius of 2′ of the peak of the X-ray emission; given the total exposure time of 7765 s, the corresponding count rate is 0.039 $\pm$ 0.003 counts s^{-1}.

As can be seen in Figure 2, NGC 1569 is immersed in a bright and morphologically complex system of Hα filaments and loops that are preferentially oriented along the optical minor axis of the galaxy (see Hunter et al. 1993 for a description of the most prominent features). In general behavior, the diffuse soft X-ray emission seems to extend preferentially along the optical minor axis of the galaxy (like the Hα emission; see also Fig. 3) and, in some locations, seems to be closely related to the filaments of Hα emission. In particular, we note the very close morphological relationship between the brightest Hα filament, which extends out $\sim$1.′3 to the west-southwest direction (Hα filament 6 in Table 3 of Hunter et al. 1993), and the spur of the X-ray emission. There is also a close morphological relationship between the Hα filament 4 in Table 3 of Hunter et al. (1993), which extends to the west-northwest direction from the nucleus, and the spur of diffuse X-ray emission extending to the north.

Approximately 2′ to the south-southeast of NGC 1569 there is a faint region of X-ray emission (this feature is also visible in Fig. 1*c* of H95). This region of soft X-ray emission is positionally consistent with the Hα filament 9 in Hunter et al. (1993). According to H95, this region has an unabsorbed 0.1–2.4 keV flux of $1.2 \pm 0.4 \times 10^{-13}$ ergs s^{-1} (assuming a count rate–to–flux conversion factor appropriate for a thermal model with $kT \sim 0.8$ keV) and, if associated with NGC 1569, a luminosity of $\sim 7 \times 10^{37}$ ergs s^{-1}.

All these similarities between the soft X-ray and the Hα emission strongly support the hypothesis that the soft X-ray emission is produced thermally by diffuse hot gas. It is now interesting to evaluate the total extent of the soft X-ray emission, as inferred from the *ROSAT* PSPC data, and to compare this extent with optical and radio size scales. In the azimuthally averaged and background-corrected radial profile, the soft X-ray emission from NGC 1569 can be detected out to a radius of $\sim$1.′9 ($\simeq$1.2 kpc) at an isophotal level of $1.3 \pm 0.6 \times 10^{-3}$ counts arcsec^{-2} ($\sim 4 \times 10^{-18}$ ergs cm^{-2} s^{-1} arcsec^{-2}) above the background. This size scale is similar to that found by H95 using the HRI data (r_{max} = 2.′0 $\simeq$ 1.25 kpc) and comparable with the standard optical isophotal radius (major axis) of the galaxy (r_{max} = 1.′8 $\simeq$ 1.13 kpc) and with the size of the nonthermal radio continuum halo (r_{max} = 1.′75 $\simeq$ 1.10 kpc). As expected from the superwind scenario, the soft X-ray emission, at the surface brightness actually sampled, derives from a region inside the overall size of the Hα filament system (r_{max} = 2.′75 $\simeq$ 1.72 kpc) and the overall extent of the H I (r_{max} = 3.′5 $\simeq$ 2.19 kpc) The half-light radius (≡the radius within which half of the total counts are contained) of the azimuthally averaged background-subtracted total X-ray emission from the *ROSAT* PSPC is $\sim$28″ ($\simeq$0.29 kpc), in very good agreement with the half-light radius estimated by H95 using the *ROSAT* HRI data ($\sim$30″ $\simeq$ 0.31 kpc) and about 2.3 times larger than the PSPC on axis PSF half-light radius ($\sim$12″). The X-ray half-light radius is comparable to the half-light radius of the Hα emission ($\sim$24″ $\simeq$ 0.25 kpc) and to that of the blue light ($\sim$26″ $\simeq$ 0.27 kpc) (see Table 3 of H95 for references to all these size scales).

In Figure 3 the contour plot of the X-ray emission is overlaid on a gray-scale representation of the POSS XE plate extracted from the digitized version available at the

PLATE 41

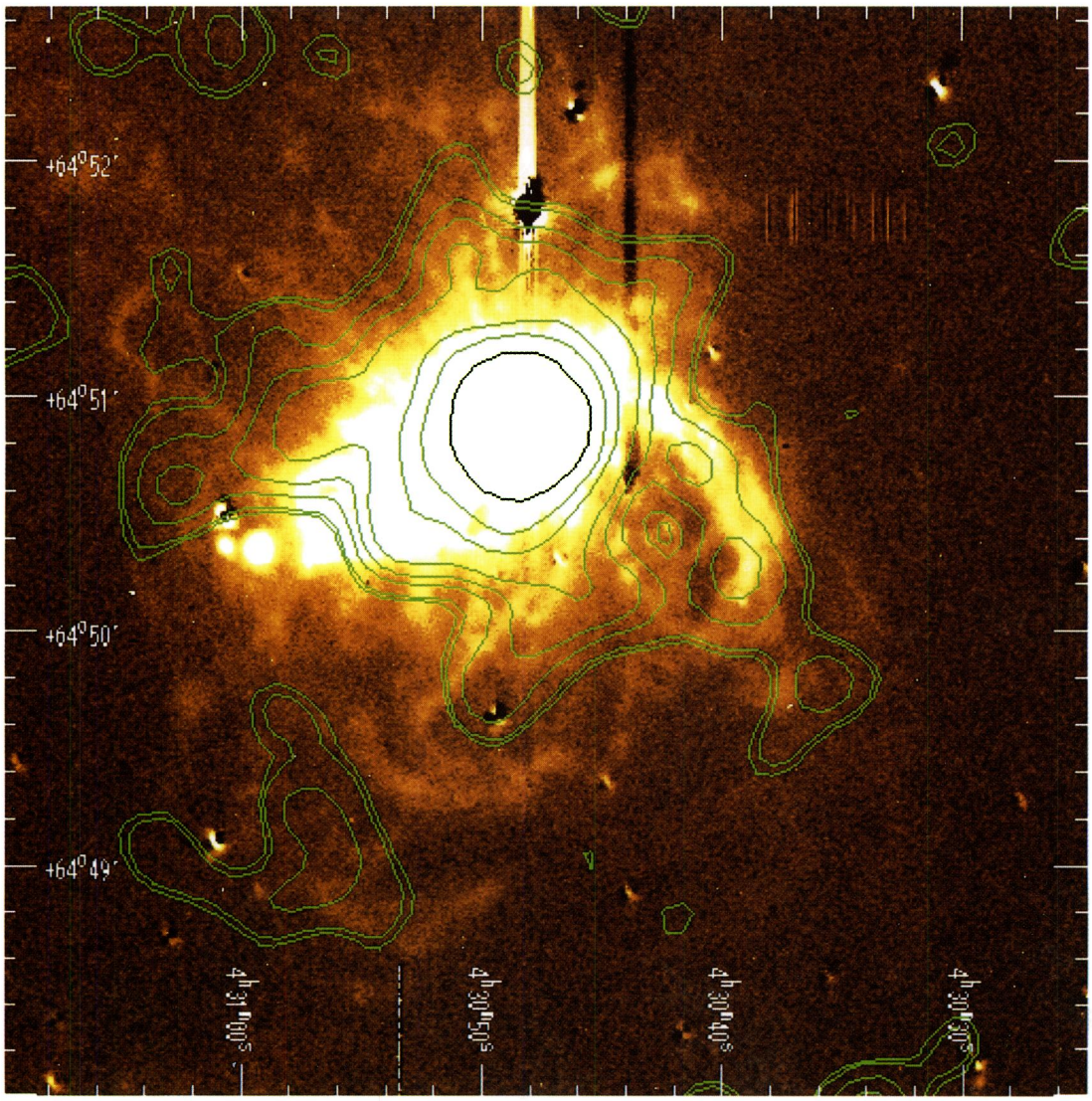

FIG. 2.—A color plot representation of the continuum-subtracted narrow-band image of the Hα emission (kindly provided by Dr. D. Hunter) with overlaid contours of the X-ray emission obtained from the smoothed *ROSAT* PSPC image of NGC 1569. The smoothed *ROSAT* PSPC image has been created from the raw PSPC data first by blocking into 4″.0 pixels, then by smoothing with a Gaussian having a FWHM ~ 19″.0. The displayed X-ray contour levels correspond to 2.5 σ, 3 σ, 5 σ, 7 σ, 10 σ, 20 σ , 30 σ, and 50 σ above the background (see § 4.2 for details).

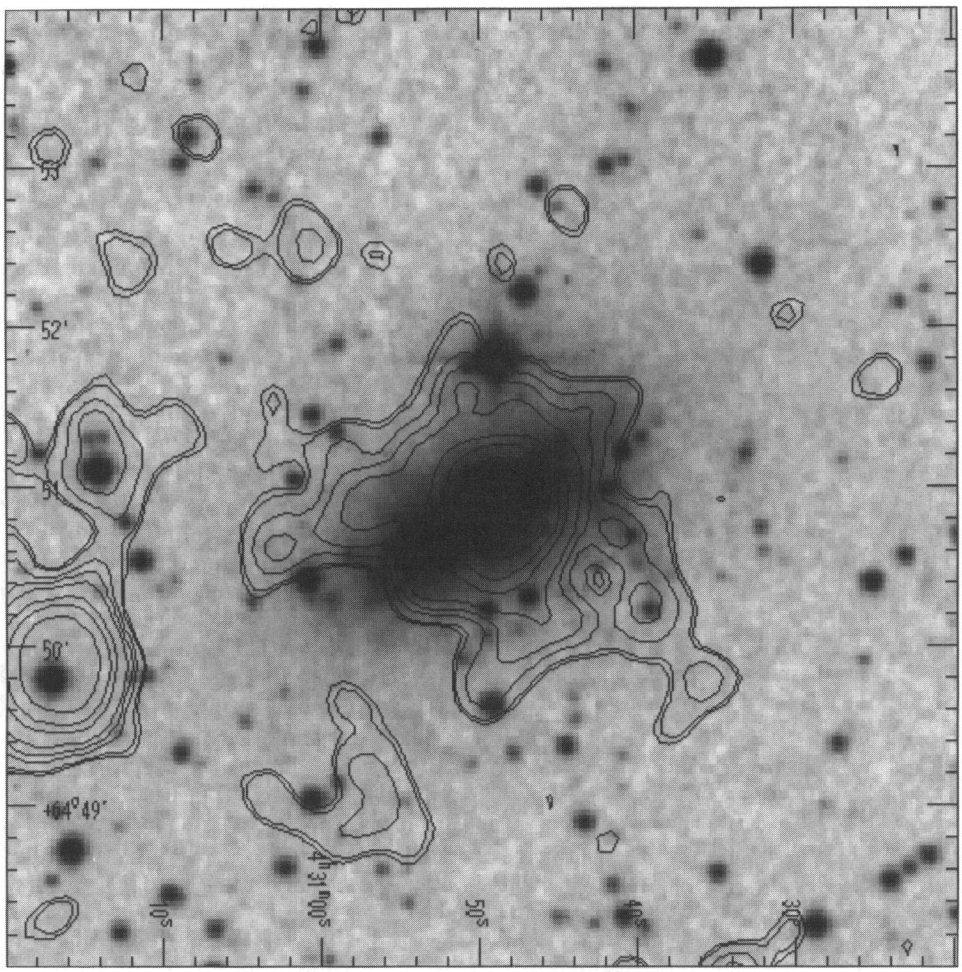

FIG. 3.—Gray-scale representation of the digitized version of the POSS XE plate with overlaid contours of the X-ray emission obtained from the smoothed *ROSAT* PSPC image of NGC 1569. The smoothed *ROSAT* PSPC image has been created from the raw PSPC data first by blocking into 4.″0 pixels and then by smoothing with a Gaussian having a FWHM ~ 19.″0. The displayed X-ray contour levels correspond to 2.5 σ, 3 σ, 5 σ, 7 σ, 10 σ, 20 σ, 30 σ, and 50 σ above the background (see § 4.2 for details).

Space Telescope Science Institute. The bright star located about 3′ to the east-southeast of NGC 1569 is apparent, along with a fainter X-ray source located above that star. The total net counts from the star are 189 ± 16 within a radius of 1.′5, about 65% of the total counts deriving from NGC 1569 itself. A similar result was obtained by H95 from the analysis of the HRI data. The total net counts from the fainter X-ray source located above the star are 19 ± 6 within a radius of ~1′, about 6% of the total counts deriving from NGC 1569. In § 5, we will show that the contamination of these two sources to the spectral results obtained for NGC 1569 is negligible.

4.3. *ASCA SIS*

The spectral analysis of the SIS data (see § 5) reveals the presence of at least two spectral components in the (0.5–6) keV broad-band X-ray emission of NGC 1569. The soft component is best described by a thermal model with a temperature of ~0.64–0.8 keV (depending on the thermal model used: i.e., the Meka thermal model or the Raymond-Smith thermal model, respectively), while the hard component can be described by a thermal model with a temperature of ~3.7 keV or by a power-law spectral model with photon index of ~2.1. Using a value of 2 keV to divide the soft and hard X-ray emission (which allows us to directly compare the soft *ASCA* SIS data with the *ROSAT* data), we find that the soft spectral component contributes ~60% at $E < 2$ keV. For $E > 2$ keV, only the hard component is expected to play a significant role. To investigate the origin and the extent of the soft and hard X-ray emission from NGC 1569, we have produced soft ($E < 2$ keV) and hard ($E > 2$ keV) SIS0 and SIS1 images. We have then used these images to determine soft and hard azimuthally averaged background-subtracted radial profiles of the X-ray emission. Because of the pointing uncertainties in the *ASCA* observations and the different positions of the source in detector coordinates in the SIS0 and SIS1 images, we cannot directly combine the two soft or the two hard X-ray images. To improve the statistics of the radial profiles, we have first analyzed the two soft (hard) X-ray images separately to determine the background-subtracted radial profiles up to ~3′. The background level of these images has been determined by calculating the mean count rate in five to six source-free regions in the same CCD chip that contains NGC 1569. We have then combined the counts in each radial bin relative to the centroid of the emission to generate a soft (hard) X-ray radial profile. In order to avoid contamination from the bright star (see § 4.2) in the radial profile, we have excluded the 90° azimuthal sector which contains this object.

In Figures 4*a* and 4*b* we show (*filled circles*) the background-subtracted radial profiles of NGC 1569 in the

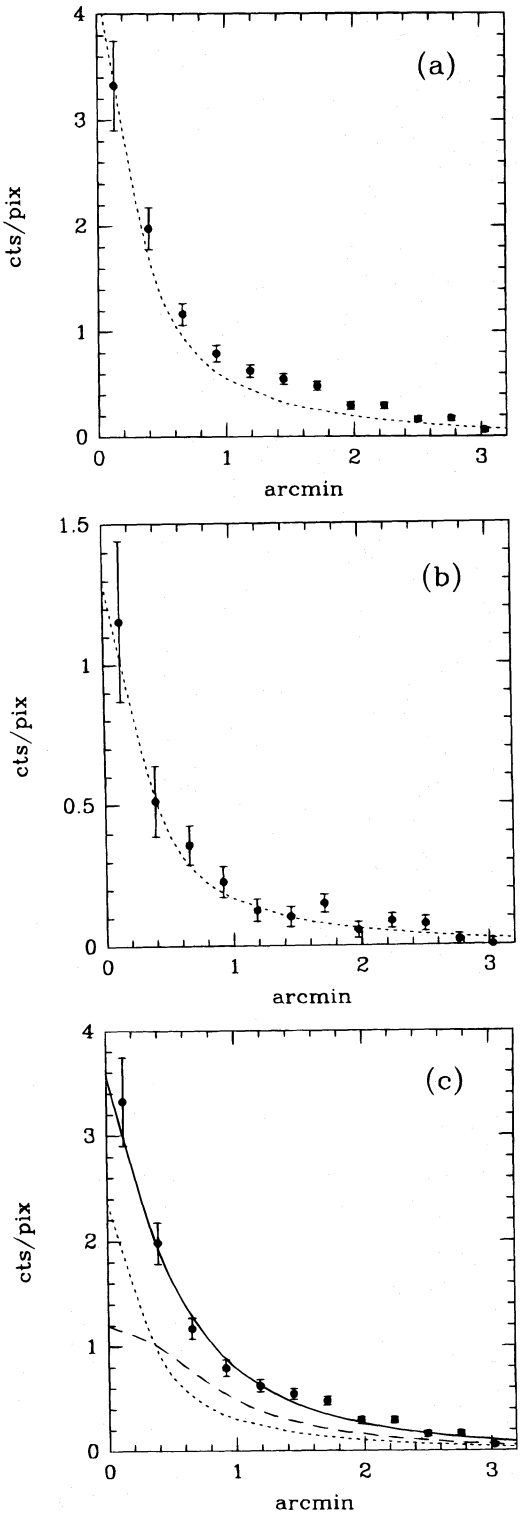

FIG. 4.—Filled dots represent the background-subtracted radial profiles of NGC 1569 in the (*a*) soft ($E < 2.0$ keV) and (*b*) hard ($E > 2$ keV) energy bands obtained using the *ASCA* SIS0 + SIS1 data. These profiles have been compared with a scaled representation of the PSF (*dotted lines*) determined from the high signal-to-noise ratio observation of 3C 273. In panel (*c*) we compare the background-subtracted radial profile of NGC 1569 in the soft band with that expected (*solid line*) from a simple model consisting of a pointlike source and diffuse X-ray emission (see § 4.3 for details). The dotted line and the dashed line indicate the contribution to the profile from the pointlike source and from the diffuse source, respectively. The bin size of the displayed profiles is ~0.′26. 1 pixel is 0.′1053 in size.

soft and hard bands, respectively. We also show (*dotted lines*) a scaled representation of the PSF. The shapes of the soft and hard PSF have been determined from the high signal-to-noise ratio observation of 3C 273 (*ASCA* Seq. ID = 70023000), which was observed as part of the Performance Verification phase of *ASCA* on 1993 June 8. Since this object was observed in 1 CCD mode, it provides an accurate in-flight measurement of the PSF at about the same position as NGC 1569 in the focal plane of the *ASCA* XRT telescope. This calibration observation was analyzed in the same way as the NGC 1569 observation. The radial profile of the hard X-ray emission is consistent with a pointlike source at the spatial resolution of the *ASCA* XRT + SIS system. On the other hand, the soft X-ray emission (Fig. 4*a*) is clearly extended, i.e., there is an evident excess of counts in the NGC 1569 data set at a distance $\gtrsim 0.'7$–$1.'0$ when compared with that expected from an unresolved source.

In order to check if the *ASCA* SIS soft X-ray profile of NGC 1569 is consistent with the results previously obtained using the *ROSAT* HRI and PSPC data (see § 4.1, § 4.2, and H95) and to obtain an estimate of the soft X-ray extent, we have assumed that the soft X-ray emission from NGC 1569 is due to the sum of a pointlike X-ray source and diffuse X-ray emission. We have modeled the diffuse X-ray emission as a bidimensional Gaussian distribution and convolved this Gaussian with the XRT + SIS PSF obtained from the *ASCA* observation of 3C 273. Because of the uncertainty in the "real" shape of the diffuse X-ray emission, we did not try a formal fit to the data, but rather we fixed the size of the bidimensional Gaussian distribution ($\sigma = 30''$, in conformance with the results obtained for the *ROSAT* PSPC and HRI) and then determined the proportions of pointlike and diffuse emissions which are consistent with the observed profile. In Figure 4*c*, we compare the background-subtracted radial profile of NGC 1569 in the soft band with that expected from this model (*solid line*), assuming that ~40% of the soft X-ray emission derives from a pointlike source and the remainder from the diffuse emission.

We would like to stress that the principal result of this analysis is the following: at the spatial resolution of the *ASCA* XRT + SIS system the soft X-ray emission is clearly extended, while the hard X-ray emission is consistent with a pointlike source. The simple model investigated for the soft X-ray emission must be considered as "consistent" with the data rather than the "best-fit" model. However, it is reassuring to note that all the X-ray size scales, along with the proportions between pointlike and diffuse emission, obtained from different detectors, are consistent with each other.

5. SPECTRAL ANALYSIS

Source counts from SIS0 and SIS1 were extracted from a circular region of ~3′ radius around the centroid of the X-ray emission from NGC 1569. This region represents the maximum allowed because of the position of NGC 1569 in the SIS0 and SIS1 CCD chips. We have also excluded from the spectral analysis a circular region of ~1.′6 radius around the star located about 3′ to the east-southeast of NGC 1569 (see § 4.2). Background counts were taken from uncontaminated regions having similar areas within the same CCD chip as that containing the NGC 1569 image. We also checked several regions for differences in the back-

ground counts but did not find any significant variations. The total net counts deriving from NGC 1569 are ~1466 (~0.019 counts s^{-1}) for SIS0 and ~1195 (~0.016 counts s^{-1}) for SIS1. The net count rate from the source must be compared with the count rate expected from the background inside the source region, that is ~0.0103 counts s^{-1} for SIS0 and ~0.0085 counts s^{-1} for SIS1. In order to use the χ^2 statistic in the spectral fitting procedure (see below), the spectra were rebinned to give at least 15 counts per bin.

A single-temperature thermal model (Raymond-Smith model or Meka model) and a simple power-law spectral model modified by Galactic absorption ($N_H = 2.1 \times 10^{21}$ cm^{-2}) were both rejected by the data at a high confidence level (≥99.99%). Allowing N_H or the abundance of the X-ray–emitting gas (in the case of the thermal models) to vary as free parameters did not produce a better fit. We then tried the following two-component models: (1) a two-temperature Raymond-Smith model (hereafter the Ray + Ray model), (2) a Raymond-Smith model combined with a power-law model (hereafter the Ray + Po model), (3) a two-temperature Meka model (hereafter the Meka + Meka model), and (4) a Meka model combined with a power-law model (hereafter the Meka + Po model). Both models were suggested from physical considerations and by the X-ray images. The soft thermal component (the Raymond-Smith thermal model or the Meka thermal model) can be associated with the halo emission seen in the PSPC image, while either the hard thermal component or the power-law component can be associated with the compact sources seen in the *ROSAT* HRI image (consistent with the assertion that they are either young supernova remnants or X-ray binaries). We have tried the two different thermal models, the Meka thermal model and the Raymond-Smith thermal model, in order to check if they give consistent results. Both of these trial spectra were filtered by photoelectric absorption due to material of solar abundance. In the spectral fits (see the discussion below), we note a correlation between the abundance of the soft X-ray–emitting gas and the best-fit spectral parameter(s) of the hard component. Since we cannot unambiguously determine the abundances in the hot gas, we have chosen to fix the metallicity at 0.25 solar, in conformity with the optically determined abundances in the nebular gas (see H95 and references therein). This is a reasonable assumption, despite the fact that the very hot gas injected by supernovae in the starburst will have a much higher metallicity. As shown by H95, the mass of the X-ray–emitting gas in NGC 1569 is so large that it must be primarily ambient interstellar gas that has been heated by the outflow. As we will argue in § 6.1 below, such an origin for the X-ray–emitting gas is also implied by its relatively low temperature ($\simeq 10^7$ K versus an expected value of $\simeq 10^8$ K for pure supernova ejecta). Thus, the abundances used to model the X-ray emission were chosen to represent the ambient interstellar medium of this galaxy. The spectral parameters of the X-ray emission do not change if we fix the N_H at the Galactic value or if we consider it as a free parameter. For this reason, in the following, we have fixed $N_H \equiv N_{H_{Gal}} = 2.1 \times 10^{21}$ cm^{-2}.

The results of the fits of the SIS0, SIS1, and the combined (SIS0 + SIS1) data set are summarized in Table 2A for the two thermal models (Ray + Ray model and Meka + Meka model) and in Table 2B for the thermal model plus the power-law model (Ray + Po model and Meka + Po model). The best-fit spectral parameters agree well within their respective 90% confidence interval, the most discordant parameter(s) being the normalizations of the soft and hard components. These different normalizations give fluxes in the 0.5–2.0 keV and in the 2–10 keV energy band that are within ~10% of the flux obtained using the best-fit spectral parameters determined from the combined (SIS0 + SIS1) data set. Since current uncertainties in expo-

TABLE 2A

RESULTS OF THE SPECTRAL FITS USING TWO THERMAL MODELS

Instruments (1)	kT_{Soft} (keV) (2)	$Norm_{Soft}$ (3)	kT_{Hard} (keV) (4)	$Norm_{Hard}$ (5)	χ^2_ν/(d.o.f.) $P(>\chi^2_\nu, \nu)$ (6)	Flux (0.5–2.0 keV) ($\times 10^{-13}$ ergs cm^{-2} s^{-1}) (7)	Flux (2.0–10.0 keV) ($\times 10^{-13}$ ergs cm^{-2} s^{-1}) (8)
Ray + Ray Model							
SIS0	$0.79^{0.85}_{0.70}$	$3.45^{4.32}_{2.49}$	$4.13^{26.4}_{2.17}$	$2.36^{3.50}_{1.56}$	1.16/60/0.20	4.24/0.68/0.32	1.95/0.10/0.90
SIS1	$0.80^{0.87}_{0.62}$	$2.16^{3.01}_{1.30}$	$3.24^{6.26}_{2.10}$	$3.34^{4.50}_{2.39}$	1.01/53/0.45	3.70/0.49/0.51	2.11/0.06/0.94
SIS0 + SIS1	$0.80^{0.85}_{0.73}$	$2.76^{3.38}_{2.12}$	$3.46^{6.10}_{2.40}$	$2.89^{3.66}_{2.20}$	1.16/117/0.15	3.95/0.58/0.42	1.99/0.08/0.92
PSPC	$0.77^{1.33}_{0.31}$	$5.56^{10.12}_{3.32}$	3.46 (fixed)	2.89 (fixed)	0.29/14/0.99	6.45/0.75/0.25	2.13/0.14/0.86
Meka + Meka Model							
SIS0	$0.64^{0.69}_{0.58}$	$4.65^{5.65}_{3.61}$	$4.94^{55.0}_{2.46}$	$2.25^{3.24}_{1.58}$	1.10/60/0.30	4.39/0.71/0.29	2.07/0.06/0.94
SIS1	$0.63^{0.72}_{0.48}$	$2.78^{3.82}_{1.60}$	$3.31^{6.67}_{2.18}$	$3.34^{4.48}_{2.40}$	1.09/53/0.30	3.78/0.49/0.51	2.13/0.04/0.96
SIS0 + SIS1	$0.64^{0.68}_{0.58}$	$3.66^{4.38}_{2.92}$	$3.81^{7.10}_{2.58}$	$2.81^{3.52}_{2.18}$	1.19/117/0.10	4.05/0.60/0.40	2.07/0.05/0.95
PSPC	$0.61^{1.14}_{0.30}$	$7.35^{11.03}_{4.05}$	3.81 (fixed)	2.81 (fixed)	0.29/14/0.99	6.66/0.76/0.24	2.15/0.09/0.91

NOTE.—The abundance in these fits has been fixed to 0.25 solar in conformance with the optically measured oxygen abundance as reported in Table 1 of H95. The absorbing column density along the line of sight has been fixed to the Galactic N_H value ($N_H = 2.1 \times 10^{21}$ cm^{-2}). Allowed ranges are 90% confidence intervals for two interesting parameters ($\chi^2_{min} + 4.61$). Columns are as follows: (1) Instrument. (2) Best-fit and 90% confidence interval of the temperature of the soft component. (3) Best-fit and 90% confidence interval of the normalization of the soft component at 1 keV in units of 10^{-4}. This number is equal to $[10^{-14}/(4\pi D^2)] \int n_e^2\, dV$, where D is the distance to the source in cm, n_e is the electron density in units of cm^{-3}, and V is the volume filled by the X-ray–emitting gas in cm^3. (4) Best-fit and 90% confidence interval of the temperature of the hard component. (5) Best-fit and 90% confidence interval of the normalization of the hard component at 1 keV in units of 10^{-4}. (6) Reduced chi-squared, degree of freedom, and the associated probability. (7) The unabsorbed flux in the (0.5–2.0) keV energy band in units of 10^{-13} ergs cm^{-2} s^{-1} and the fractional contribution to this flux from the soft and the hard component. (8) The unabsorbed flux in the (2.0–10.0) keV energy band in units of 10^{-13} ergs cm^{-2} s^{-1} and the fractional contribution to this flux from the soft and the hard component.

TABLE 2B

RESULTS OF THE SPECTRAL FITS USING THE THERMAL MODEL PLUS THE POWER-LAW MODEL

Instruments (1)	kT_{Soft} (keV) (2)	$Norm_{Soft}$ (3)	kT_{Hard} (keV) (4)	$Norm_{Hard}$ (5)	χ^2_ν/(d.o.f.) $P(>\chi^2_\nu, \nu)$ (6)	Flux (0.5–2.0 keV) ($\times 10^{-13}$ ergs cm^{-2} s^{-1}) (7)	Flux (2.0–10.0 keV) ($\times 10^{-13}$ ergs cm^{-2} s^{-1}) (8)
Ray + Po Model							
SIS0	$0.79^{0.85}_{0.69}$	$2.90^{3.90}_{1.97}$	$2.18^{2.55}_{1.67}$	$0.91^{1.29}_{0.52}$	1.07/60/0.30	4.49/0.55/0.45	1.97/0.08/0.92
SIS1	$0.82^{0.90}_{0.65}$	$1.86^{2.75}_{0.98}$	$2.15^{2.43}_{1.81}$	$1.11^{1.46}_{0.75}$	0.95/53/0.50	3.99/0.39/0.61	2.42/0.05/0.95
SIS0 + SIS1	$0.80^{0.86}_{0.73}$	$2.34^{3.01}_{1.71}$	$2.17^{2.39}_{1.89}$	$1.02^{1.27}_{0.75}$	1.09/117/0.25	4.21/0.46/0.54	2.20/0.07/0.93
PSPC	$0.78^{1.57}_{0.30}$	$5.18^{9.79}_{2.90}$	2.17 (fixed)	1.02 (fixed)	0.29/14/0.99	6.69/0.66/0.34	2.35/0.12/0.88
Meka + Po Model							
SIS0	$0.63^{0.69}_{0.57}$	$4.14^{5.37}_{2.91}$	$2.00^{2.42}_{1.43}$	$0.79^{1.19}_{0.41}$	1.06/60/0.35	4.54/0.61/0.39	2.18/0.05/0.95
SIS1	$0.65^{0.78}_{0.49}$	$2.32^{3.49}_{1.09}$	$2.13^{2.42}_{1.77}$	$1.13^{1.50}_{0.74}$	1.05/53/0.40	4.02/0.39/0.61	2.45/0.03/0.97
SIS0 + SIS1	$0.64^{0.69}_{0.59}$	$3.14^{4.00}_{2.31}$	$2.09^{2.34}_{1.79}$	$0.97^{1.24}_{0.70}$	1.14/117/0.15	4.24/0.49/0.51	2.29/0.04/0.96
PSPC	$0.62^{1.38}_{0.29}$	$6.87^{10.50}_{3.60}$	2.09 (fixed)	0.97 (fixed)	0.29/14/0.99	6.86/0.68/0.32	2.37/0.08/0.92

NOTE.—The abundance in these fits has been fixed to 0.25 solar in conformance with the optically measured oxygen abundance as reported in Table 1 of H95. The absorbing column density along the line of sight has been fixed to the Galactic N_H value ($N_H = 2.1 \times 10^{21}$ cm^{-2}). Allowed ranges are 90% confidence intervals for two interesting parameters ($\chi^2_{min} + 4.61$). Columns are as follows: (1) Instrument. (2) Best-fit and 90% confidence interval of the temperature of the soft component. (3) Best-fit and 90% confidence interval of the normalization of the soft component at 1 keV in units of 10^{-4}. This number is equal to $[10^{-14}/(4\pi D^2)] \int n_e^2\, dV$, where D is the distance to the source in cm, n_e is the electron density in units of cm^{-3}, and V is the volume filled by the X-ray–emitting gas in cm^3. (4) Best-fit and 90% confidence interval of the power-law photon index. (5) Best-fit and 90% confidence interval of the normalization of the power-law component in units of 10^{-4} keV^{-1} s^{-1} cm^{-2} keV^{-1} at 1 keV. (6) Reduced chi-squared, degree of freedom, and the associated probability. (7) The unabsorbed flux in the (0.5–2.0) keV energy band in units of 10^{-13} ergs cm^{-2} s^{-1} and the fractional contribution to this flux from the soft and the hard component. (8) The unabsorbed flux in the (2.0–10.0) keV energy band in units of 10^{-13} ergs cm^{-2} s^{-1} and the fractional contribution to this flux from the soft and the hard component.

sure corrections make it difficult to obtain absolute SIS fluxes (see also the discussion below), we have considered in the following the mean normalization obtained from the combined (SIS0 + SIS1) data set.

The unfolded and folded spectra of the combined SIS0 + SIS1 data set are shown in Figure 5 and Figure 6, respectively. In Figure 6, we also show the residuals of the fit. The spectra reported in both figures refer to the case of the Meka + Meka model, but very similar results are obtained for the other spectral models.

The probabilities summarized in Table 2A and Table 2B indicate that both of the two-component models are a good representation of the current data set. The broad band (0.5–6 keV) X-ray spectrum of NGC 1569 thus reveals the pres-

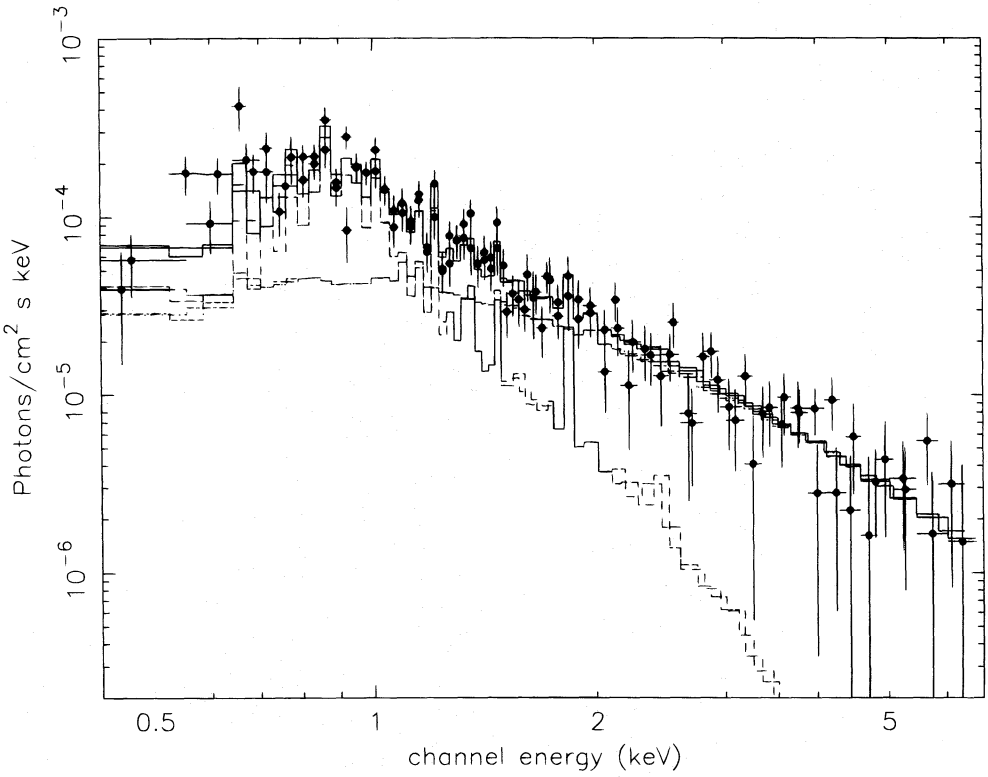

FIG. 5.—*ASCA* (SIS0 + SIS1) unfolded spectrum of NGC 1569 fitted with the two-temperature Meka model (Meka + Meka model)

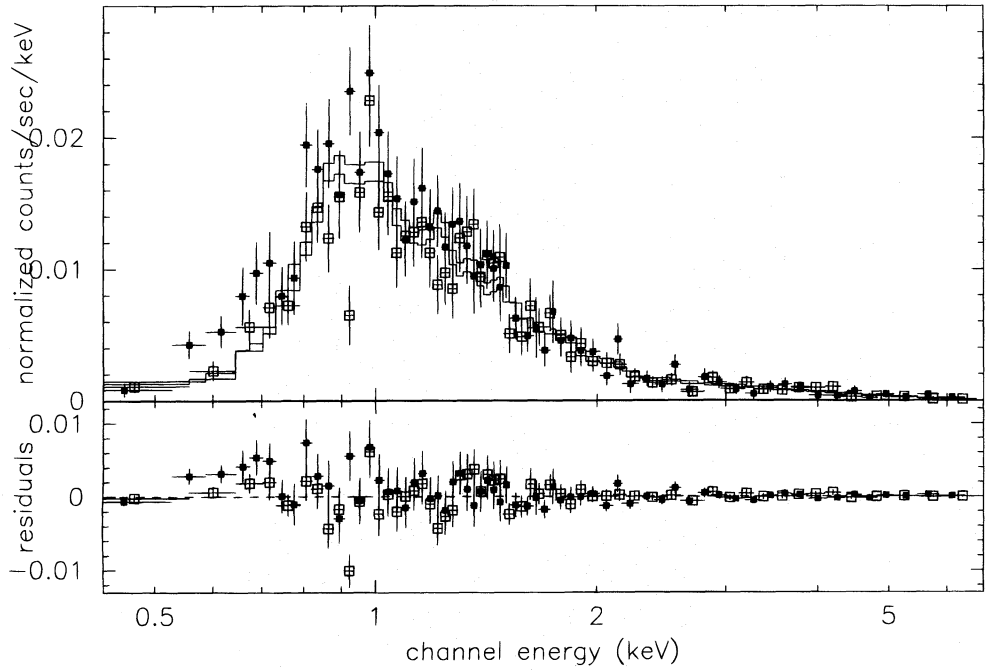

FIG. 6.—*ASCA* (SIS0: *open squares* + SIS1: *filled squares*) folded spectrum of NGC 1569 (fitted with the two-temperature Meka model) and the residuals of the fit.

ence of at least two spectral components; the soft component is best described by a Meka (Raymond-Smith) thermal model with a temperature of $\sim$0.64 ($\sim$0.8) keV, while the hard component can be described by a thermal model with a temperature of $\sim$3.7 keV or by a power-law spectral model with photon index of $\sim$2.1.

From the residual of the best fit Meka + Meka model (see Fig. 6), we note an excess of counts around 0.6–0.7 keV. This is a common feature of all our best fit spectral models reported in Table 2A and Table 2B, and it is also found when we consider the $N_{\rm H}$ as a free parameter. Because of the extant calibration problems at these energies, due to the ill-defined modeling of the O K-edge in the *ASCA* SIS response matrices, it is premature to consider this discrepancy as an indication of a more complex spectrum. However, it is worth noting that we clearly detect a very soft thermal component ($kT \sim 0.2$–0.3 keV) in the joint *ASCA* + PSPC spectrum of the low-luminosity star-forming galaxy NGC 4449 (Della Ceca et al. 1996) that has optical and X-ray properties very similar to NGC 1569. The high Galactic column density along the line of sight to NGC 1569 ($N_{\rm H_{gal}} = 2.1 \times 10^{21}$ cm^{-2}) could prevent us from clearly detecting this very soft component.

As discussed in § 4.2, a bright X-ray–emitting star is located about 3′ to the east-southeast of NGC 1569. In order to evaluate the possible contamination from this object, we have integrated the counts within a radius of $\sim$3′ around the centroid of the X-ray emission from NGC 1569, but excluding now a circular region of 3.′16 radius around the centroid of the X-ray emission from the star. For a pointlike source, a circular region of 3.′16 radius should contain about 85% of the photons from the source. The best-fit spectral parameters of the X-ray emission obtained using this new data set are in excellent agreement with the spectral parameters previously determined, confirming that the contamination from the star, if any, is negligible.

We have also investigated the dependence of the derived spectral parameter(s) on the abundance of the X-ray–emitting gas. Fixing the abundance at different values in the range 0.05–1.0 solar, we find that the temperature of the soft component does not change. On the contrary, we note a correlation between the best-fit spectral parameter(s) of the hard component and the abundance of the X-ray–emitting gas. In particular, we note a flattening of the hard component as the abundance is lowered. For example, in the case of the Ray + Po model, the best-fit photon spectral index of the power-law component is $\Gamma \sim 2.3$ if the abundance of the X-ray–emitting gas is fixed at the solar value and $\Gamma \sim 1.4$ if the abundance of the X-ray–emitting gas is fixed at 0.05 solar. In the case of the Ray + Ray model, the best-fit temperature of the hard component is $kT \sim 3.5$ keV if the abundance of the X-ray–emitting gas is fixed at the solar value and $kT \sim 20$ keV if the abundance is 0.05 solar.

We shall now investigate if the PSPC data are consistent with these spectral models. Source counts from the *ROSAT* PSPC were extracted from a circular region of $\sim$2′ radius around the centroid of the X-ray emission from NGC 1569. The background data were taken from an uncontaminated region close to NGC 1569. A total of 300 $\pm$ 20 net counts were obtained from the source. Because of the poor statistics and the limited energy range of the *ROSAT* PSPC, we did not try to fit the overall spectral shape; instead, we have fixed the spectral parameters of the hard component from the SIS0 + SIS1 data set, the absorbing column density at the Galactic value, and then determined the best-fit spectral parameters of the soft component. The results of these spectral fits are also reported in Table 2A (Ray + Ray model and Meka + Meka model) and Table 2B (Ray + Po model and Meka + Po model). As can be seen, the best-fit temperature of the soft component is in excellent agreement with that derived using the *ASCA* data. However, there is disagreement between the normalization of the soft com-

ponent determined from the *ASCA* (SIS0 + SIS1) data set and that determined from the *ROSAT* PSPC data set. The normalization of the soft component obtained from the *ROSAT* PSPC best-fit model is about a factor 2 greater than that determined from the (SIS0 + SIS1) best-fit model. A similar disagreement has been recently pointed out by Nandra (1995) by comparing simultaneous *ASCA* and *ROSAT* PSPC observations of the Seyfert 1.5 galaxy NGC 5548. The best-fit PSPC spectra of this object produce a 0.4–2.0 keV flux that is about 1.5 times higher than that obtained from the *ASCA* (SIS0 + SIS1) data set; the two data sets became compatible for energy above $\sim$1.5 keV. The larger discrepancy in the case of NGC 1569 is probably due to the size of our extraction region ($\sim$3′ radius), which is more appropriate for a pointlike source. Unfortunately, being limited by the boundary of the chips, we can not use a larger extraction radius. Using our simple model, which describes the soft X-ray emission profile of NGC 1569 (see § 4.3), we can estimate that the extraction radius we used encloses $\sim$70% of the soft ($E < 2$ keV) photons deriving from the diffuse source.

Assuming a mean value (between the *ASCA* SIS0 + SIS1 data set and the *ROSAT* PSPC data set) for the normalization of the soft component, the 0.2–4.0 keV unabsorbed flux is $\simeq 9.0 \times 10^{-13}$ ergs cm^{-2} s^{-1}. This value is lower than that previously determined from Fabbiano, Kim, & Trinchieri (1992) using data from the Imaging Proportional Counter (IPC) on board the *Einstein Observatory* [f_X (0.2–4 keV) = $1.9 \pm 0.2 \times 10^{-12}$ ergs cm^{-2} s^{-1} for a conversion factor appropriate for a 5 keV thermal model]. Taking into account the fact that the IPC flux also contains the bright star located about 3′ to the east-southeast of NGC 1569 (the count rate from this star is $\sim$65% of the count rate from NGC 1569 itself) and considering the problems we have discussed above on the absolute flux of our observations, the agreement between our flux and the IPC flux can be considered satisfactory.

Using the same mean normalization for the soft component, the unabsorbed fluxes (luminosities) in the 0.5–2.0 keV and in the 2–10 keV energy band are f_X (0.5–2.0 keV) $\simeq 5.4 \times 10^{-13}$ ergs cm^{-2} s^{-1} [L_X (0.5–2.0 keV) $\simeq 3.1 \times 10^{38}$ ergs s^{-1}] and f_X (2.0–10.0 keV) $\simeq 2.2 \times 10^{-13}$ ergs cm^{-2} s^{-1} [L_X (2.0–10.0 keV) $\simeq 1.3 \times 10^{38}$ ergs s^{-1}], respectively; the soft thermal component provides $\sim$60% of the total flux in the 0.5–2.0 keV energy band but less than 10% of the total flux in the 2–10 keV energy band.

Based on the different normalizations of the soft component (the *ASCA* SIS0 + SIS1 normalization or the *ROSAT* PSPC normalization) and on the different best-fit spectral models, we have estimated that the above reported fluxes and luminosities in the 0.2–4.0 keV and in the 0.5–2.0 keV energy band are accurate to $\pm$30%. The fluxes and luminosities in the 2–10 keV energy band are accurate to $\pm$15%. We will show in the next section that this uncertainty on the absolute flux scale does not influence our conclusions.

6. DISCUSSION

6.1. *The Origin of the Soft X-Ray Emission and Its Relevance to Starburst-driven Outflows*

As discussed by H95, optical imaging and long-slit spectroscopy of NGC 1569 demonstrate the presence of a large-scale outflow in the interstellar medium. The *ROSAT* HRI X-ray image presented by H95 suggested that this outflow was being driven by a piston of hot gas created by the combined energy input of the multiple supernovae in the central starburst. The *ROSAT* PSPC and especially the new *ASCA* data presented in this paper confirm and extend these results in several important ways.

First, they show unambiguously that the X-ray halo in NGC 1569 is thermal emission from hot gas and not inverse-Compton emission from the relativistic electrons in the radio synchrotron halo. H95 had made only indirect arguments in favor of thermal emission. Thus, a basic element of the starburst-driven outflow scenario is confirmed.

Second, the measured temperature of the halo allows us now to determine the physical properties of the X-ray halo. H95 derived these properties but had to assume a temperature to do so. We measure a temperature of 0.64–0.8 keV (depending on the thermal model; see § 5), and an implied emission integral ($\equiv \int n_e^2\, dV$, where n_e is the electron density in units of cm^{-3} and dV is the volume filled from the X-ray–emitting gas) of 1.7×10^{61} cm^{-3} for the *ASCA* normalization and 3.6×10^{61} cm^{-3} for the *ROSAT* PSPC normalization (see § 5 and Table 2A and Table 2B). For consistency, we adopt the same geometry as H95 for the X-ray emission, namely a source volume of 1.23×10^{65} cm^3, corresponding to a sphere of radius 1 kpc. Parameterizing the volume-filling factor of the hot gas as f, the basic physical properties of the X-ray halo are an electron density of $1.2 \times 10^{-2} f^{-1/2}$ cm^{-3}, a pressure of 2.7×10^{-11} $f^{-1/2}$ dyne cm^{-2}, a mass of $1.2 \times 10^6 f^{1/2}$ $M_\odot$, a thermal energy of $5 \times 10^{54} f^{1/2}$ ergs, and a radiative cooling time of $3 \times 10^8 f^{1/2}$ yr. These estimates assume the *ASCA* normalization. If the *ROSAT* PSPC normalization is adopted, all the above quantities increase by a factor 1.46 (except for the cooling time, which decreases by this same factor).

These physical quantities are similar to those estimated by H95, who show that they can be readily understood in the context of X-ray emission from the interior of a wind-driven bubble that has been blown over the past $\sim 10^7$ yr by the mechanical energy injected by the starburst ($L_{\rm mech} \sim 10^{41}$ ergs s^{-1}) and which expands into the galaxy's H I envelope at about 100 km s^{-1}. The thermalization of pure supernova ejecta produces gas with a characteristic temperature $\sim 10^8$ K (see Chevalier & Clegg 1985). Thus, the much lower temperature we measure ($\sim 10^7$ K) implies that the X-ray–emitting gas in NGC 1569 is not pure supernova ejecta but has instead been strongly contaminated by the evaporation of ambient interstellar matter. This is consistent with the inferences made by H95 on the basis of the X-ray luminosity.

Finally, the new X-ray data allow us to revisit the question as to the fate of the hot outflowing gas in NGC 1569. While H95 were able to show that NGC 1569 was driving an outflow, they were not able to determine unambiguously whether the observed outflow was rapid enough to escape from the galaxy's potential well. This issue is particularly important in assessing the role of starburst-driven outflows in the evolution of dwarf galaxies and on the chemical enrichment of the intergalactic medium.

To address this question, we follow Wang et al. (1995) and use Bernoulli's theorem to relate the "escape temperature" for hot gas in a galaxy potential to the escape velocity (assuming an adiabatic and approximately steady

flow along streamlines):

$$T_{es} \simeq (10^5 \times v_{es}/84 \text{ km s}^{-1})^2 \text{ K} .$$

The H I rotation curve in NGC 1569 peaks at 33 km s^{-1} (Reakes 1980). If there is no dark matter halo, the estimated escape velocity (see eq. [13] in H95) at a radius of 1.7 kpc (the radius of the optical filament system) is about 47 km s^{-1}. If NGC 1569 has an isothermal dark halo that extends out to 20 times the optical Holmberg radius (i.e., out to $\sim$20 kpc), the escape velocity at a radius of 1.7 kpc is 87 km s^{-1}. The implied values of T_{es} are 3×10^4 K and 1.1×10^5 K, respectively. Comparing these to the measured temperature of the hot gas ($\sim 10^7$ K), we conclude that the observed gas can easily escape from the galaxy unless it suffers strong radiative cooling. As argued by H95, this possibility is unlikely: the estimated radiative cooling time is an order of magnitude longer than the gasdynamical timescale, and the observed X-ray luminosity is about 2 orders of magnitude less than the rate at which the gas is being heated by the starburst's supernovae. Moreover, the size of the X-ray halo is only slightly less than that of the Hα envelope in which it appears to be embedded. This suggests that the hot gas should soon "blow out" of the interstellar medium. The escape of the hot gas has very interesting consequences, since this gas will carry with it a substantial fraction of the metals created in the starburst. Such a process has been hypothesized to explain both the low observed metal abundances in dwarf galaxies and the chemical enrichment of the intergalactic medium (see Dekel & Silk 1986).

It is more difficult to determine whether the observed outflow in NGC 1569 will lead to the removal of most of the interstellar medium. If it can, it may be possible to shut off future star formation, allowing NGC 1569 to fade and redden. This scenario forms the basis of models that propose that star-forming dwarf galaxies like NGC 1569 can be transformed into dwarf elliptical galaxies in the aftermath of a starburst and is also invoked in models like those of Babul & Ferguson (1996) in which the observed population of faint blue galaxies at intermediate redshifts self-destructs via wind-driven mass loss. H95 show that the amount of kinetic energy provided by the starburst is large enough in principle to unbind the observed H I gas. However, this simple estimate does not take the nonspherical or multiphase nature of the ISM into account, both of which tend to make it more difficult to blow away the interstellar medium (see De Young & Heckman 1994; Hensler, Theis, & Burkert 1993). Thus, the hot gas may be able to vent out into the intergalactic medium, carrying the newly created metals with it, but leaving the galaxy's H I disk intact but tattered.

6.2. *The Origin of the Hard X-Ray Emission and Its Relevance to the Cosmic X-Ray Background*

As discussed in § 4.3, the hard ($E > 2$ keV) X-ray emission deriving from NGC 1569 is consistent with a pointlike source at the spatial resolution of the *ASCA* XRT + SIS system. In § 5, we have also shown that the soft X-ray spectral component should play a marginal role at these energies. Therefore, the hard X-ray component is expected to derive from the central starburst that we have imaged with the *ROSAT* HRI at soft energies (see Fig. 1). If this picture is correct, the unabsorbed flux in the 0.1–2.4 keV energy band deriving from the hard spectral component should be consistent with the integrated flux of the bright knots of X-ray emission that we see in the *ROSAT* HRI image. The unabsorbed flux in the 0.1–2.4 keV energy band of the hard spectral component is $\simeq 2.7 \times 10^{-13}$ ergs cm^{-2} s^{-1} in the case of the hard thermal ($kT \sim 3.7$) component and $\simeq 5.6 \times 10^{-13}$ ergs cm^{-2} s^{-1} in the case of the power-law ($\Gamma \sim 2.1$) spectral component. On the assumption of a count rate–to–flux conversion factor appropriate for a hot thermal model ($kT \sim 5$ keV), H95 estimate unabsorbed 0.1–2.4 keV X-ray fluxes of $\simeq 2.2 \times 10^{-13}$ ergs cm^{-2} s^{-1} and $\simeq 1.1 \times 10^{-13}$ ergs cm^{-2} s^{-1} for the two brightest blobs of X-ray emission visible in Figure 1. The 0.1–2.4 keV flux deriving from the hard spectral component is then consistent with the flux in the two brightest knots of X-ray emission visible in Figure 1. Under this hypothesis and assuming the same flux proportional factor that we measure at soft X-ray energies, we estimate 2–10 keV fluxes (luminosities) of $\simeq 1.3 \times 10^{-13}$ ergs cm^{-2} s^{-1} ($L_X \simeq 7.6 \times 10^{37}$ ergs s^{-1}) and $\simeq 0.7 \times 10^{-13}$ ergs cm^{-2} s^{-1} ($L_X \simeq 4.0 \times 10^{37}$ ergs s^{-1}) for these two sources.

Three classes of compact X-ray sources could have luminosities of this order of magnitude: low-mass X-ray binaries, high-mass X-ray binaries, and young supernova remnants. However, the spectral shape we observe for the hard spectral component is more typical of low-mass X-ray binaries ($kT \sim 5$–9 keV) or young supernova remnants ($kT \sim 2$–3 keV) rather than high-mass X-ray binaries ($kT \gtrsim 15$ keV), which are expected as natural evolutionary end points of the massive stars formed in the starburst (see Petre 1993 and references therein). The timescale for formation of low-mass X-ray binaries argues in favor of the young supernova remnant.

Based on the observed correlation between X-ray and infrared luminosity of a sample of starburst galaxies and on the hypothesis that their hard ($E > 2$ keV) X-ray emission is dominated by massive X-ray binaries in regions of low metallicity (like the massive X-ray binaries in the Magellanic Clouds) many authors (see, e.g., Griffiths & Padovani 1990; Green, Anderson, & Ward 1992; David, Jones, & Forman 1992; Treyer et al. 1992) have pointed out that such starburst galaxies could also make a significant contribution to the hard ($E > 2$ keV) X-ray background ($\sim$a few tens of percent up to at least 10 keV or even 20 keV). We do not see the very hard ($kT > 15$ keV) spectral component, typical of massive X-ray binaries in regions of low metallicity, in the *ASCA* spectra of NGC 1569. If we consider NGC 1569 as a prototype of the blue star-forming dwarf galaxy population contributing to the faint blue number counts (see, e.g., Broadhurst, Ellis, & Shanks 1988; Cowie 1991; Babul & Rees 1992; Glazebrook et al. 1995; Driver et al. 1995a, 1995b; Babul & Ferguson 1996; Saracco, Chincarini, & Iovino 1996), then we do not expect a large contribution from these objects to the hard X-ray background.

These conclusions, that the more probable origin of the hard component is in low-mass X-ray binaries or young supernova remnants and that these objects do not contribute significantly to the hard X-ray background, could depend on the assumed abundance of the soft X-ray–emitting gas. We have used an abundance equal to 0.25 solar, in conformance with the optically measured oxygen abundance as reported in Table 1 of H95, but as discussed in § 5, we note a correlation between the best-fit spectral parameter(s) of the hard component and the abundance of

the X-ray emitting gas. If the abundance of the soft X-ray emitting gas were about a factor of 3 lower than that assumed here, then the spectral parameter(s) of the hard component could become consistent with those observed in high-mass X-ray binaries. Such a hard component could became relevant, in our case, for energies greater than ~ 6 keV. If this is the case, then objects like NGC 1569 could play some role also in the production of the hard X-ray background.

7. SUMMARY AND CONCLUSION

We have presented *ASCA* observations of the nearby starbursting dwarf galaxy NGC 1569. Combining the *ASCA* data with archival *ROSAT* PSPC and HRI data, we have been able to investigate the X-ray emission at different physical scales (from ~ 0.1 to ~ 3 kpc for an assumed distance of 2.2 Mpc) as well as the spectral emission characteristics of this object over about a factor 12 in energy (from ~ 0.5 to ~ 6 keV). We have compared these X-ray data with optical broad-band and narrow-band Hα images and new infrared K-band images. We summarize below the X-ray properties of NGC 1569 taking into account these new data and considering the specific aims of this investigation discussed in § 1.

The broad-band (0.5–6 keV) X-ray spectrum of NGC 1569 is complex and reveals the presence of at least two spectral components. The soft component is best described by a thermal model with $kT \sim 0.64$–0.8 keV (depending on the thermal emission code; i.e., the Meka thermal model or the Raymond-Smith thermal model), while the hard component can be described by a thermal model with $kT \sim 3.7$ or by a power-law spectral model with photon index of ~ 2.1. The total X-ray luminosity of NGC 1569 is $\sim 3.1 \times 10^{38}$ ergs s^{-1} in the 0.5–2.0 keV energy band and $\sim 1.3 \times 10^{38}$ ergs s^{-1} in the 2–10 keV energy band. The soft thermal component provides $\sim 60\%$ of the total luminosity in the 0.5–2.0 keV energy band but less than $\sim 10\%$ of the total luminosity in the 2–10 keV energy band. From the residual of the best-fit model(s), we also have some indication for the presence of a very soft thermal component ($kT \sim 0.2$–0.3), but because of the extant calibration problems in the *ASCA* SIS response matrices around 0.6 keV and the high Galactic column density along the line of sight ($N_{\rm H_{gal}} = 2.1 \times 10^{21}$ cm^{-2}), we cannot clearly detect this very soft component. Similar spectral components are found to describe the *ASCA* spectrum of larger starburst galaxies (e.g., M82 and NGC 253; Awaki et al. 1995), which suggests that the underlying processes at work may be the same. The soft thermal components in these larger starburst galaxies are extended and are interpreted as deriving from the galactic superwind triggered by starburst activity.

About 60% of the soft ($E < 2$ keV) X-ray emission is clearly diffuse and can be detected up to ~ 1.2 kpc from the central starburst of NGC 1569. It seems to extend preferentially along the optical minor axis of the galaxy (as does the Hα emission) and, in some locations, seems to be closely related to the filaments of Hα emission. These features are predicted in the superwind scenario, in which the hot gas produced from the starburst activity is expected to expand most rapidly along the direction of the steepest pressure gradient of the ISM (i.e., the optical minor axis) and to shock-heat the dense interstellar or circumgalactic gas causing it to emit optical line radiation. The HRI image shows that the remainder of the soft X-ray emission arises in a knotty region several hundred parsecs in size positionally coincident with the central starburst. The hard ($E > 2$ keV) X-ray emission is consistent with a pointlike source (the central starburst) at the spatial resolution of the *ASCA* XRT + SIS system.

All the properties of the soft X-ray emission strongly support the suggestion of H95 that a piston of hot gas is driving a large-scale outflow in the interstellar medium. Using these new data, we have been able to confirm, extend, and strengthen the results already obtained by H95 in several important points. We show unambiguously that the X-ray halo in NGC 1569 is thermal emission from hot gas, confirming a basic element (the "piston") of the starburst-driven outflow. The physical properties of the soft X-ray–emitting halo, as derived from our best-fit spectra, are very similar to those predicted by H95 in the context of X-ray emission from the interior of a wind-driven bubble that has been blown over the past $\sim 10^7$ yr by the mechanical energy injected by the starburst ($L_{\rm mech} \sim 10^{41}$ ergs s^{-1}) and which expands into the galaxy's H I envelope at about 100 km s^{-1}.

This galactic superwind could have a devastating impact on the evolution of dwarf galaxies, because their low escape velocity could allow the removal of substantial amounts of interstellar matter. This would have a major bearing on the disappearance of faint blue dwarfs between moderate redshift ($z \sim 0.1$) and the local universe, on the chemical enrichment of the intergalactic medium, and on the low observed metal abundance in dwarf galaxies. We have shown that, in the case of NGC 1569, the hot outflowing gas can easily escape from the galaxy, carrying with it a substantial fraction of the metals created in the starburst. To understand if the observed outflow in NGC 1569 will lead to the removal of most of the interstellar medium is more difficult. This possibility, although energetically feasible (see H95 for a discussion of this point), strongly depends on the nonspherical or multiphase nature of the ISM.

The most probable origin of the hard component ($kT \sim 3.7$ keV) is the starburst itself; almost all the flux of the hard component could be associated with the two brightest knots of X-ray emission that we see in the *ROSAT* HRI image. If this is the case, then the luminosity and the spectral shape indicate that these two objects could be low-mass X-ray binaries or young supernovae remnants.

Finally, if the spectral shape we have found for NGC 1569 is typical of dwarf star-forming galaxies, then their spectral energy distribution is not appropriate for the production of the spectrum of the hard (>2 keV) X-ray background. These objects contribute in a major way to the soft X-ray background only.

We are grateful to D. Hunter, who provided us with the continuum-subtracted narrow-band image of the Hα shown in Figure 2, and to K. Weaver for helpful discussions. We acknowledge partial support from NASA grants, NAGW-3138, NAG 5-2728, and NAGW-2131. We would like to thank the staff of the Laboratory for High Energy Astrophysics (LHEA) at NASA/GSFC for their efforts to maintain the *ROSAT* and *ASCA* archive. This research has made use of the NASA/IPAC extragalactic database (NED) which is operated by the Jet Propulsion Laboratory, Caltech, under contract with the National Aeronautics and Space Administration.

REFERENCES

Abraham, R. G., van den Bergh, S., Glazebrook, K., Ellis, R. S., Santiago, B. X., Surma, P., & Griffiths, R. 1996, ApJS, in press
Arnaud, K. A.. 1996, in Astronomical Data Analysis Software and Systems V, ed. G. Jacoby & J. Barnes, in press
Awaki, H., et al. 1995, in Proc. Eleventh Symp. on UV and X-Ray Spectroscopy of Astrophysical and Laboratory Plasmas (Tokyo: Universal Academy), in press
Babul, A., & Ferguson H. C. 1996, ApJ, 458, 100
Babul, A., & Rees, M. J. 1992, MNRAS, 255, 346
Binggeli, B. 1994, in Panchromatic View of Galaxies: Their Evolutionary Puzzle, ed. G. Hensler, C. Theis, & J. Gallagher (Gif-sur-Yvette: Editions Frontières), 172
Blackburn, J. K., Brown, L. E., Greene, E. A., & Tripicco, M. J. 1995, Users' Guide to FTOOLS (Greenbelt: NASA/GSFC)
Blumenthal, G. R., Faber, S. M., Primack, J. R., & Rees, M. J. 1984, Nature, 311, 517
Broadhurst, T., Ellis, R. S., & Shanks, T. 1988, MNRAS, 235, 827
Chevalier, R., & Clegg, A. 1985, Nature, 317, 44
Cowie, L. L. 1991, Phys. Scr., T36, 102
Cowie, L. L., Hu, E. M., & Songaila, A. 1995, Nature, 377, 603
David, L. P., Harnden, F., Kearns, K., & Zombek, M. 1993, The *ROSAT* High Resolution Imager (Cambridge: Harvard-Smithsonian Center for Astrophysics)
David, L. P., Jones, C., & Forman, W. 1992, ApJ, 369, 121
Day, C., Arnaud, K., Ebisawa, K., Gotthelf, E., Ingham, J., Mukai, K., & White, N. 1995, The ABC Guide to *ASCA* Data Reduction (Greenbelt: NASA/GSFC)
Dekel, A., & Silk, J. 1986, ApJ, 303, 39
Della Ceca, R., et al. 1996, in preparation
de Vaucouleurs, G., de Vaucouleurs, A., Corwin, H. Buta, R., Paturel, R., & Fouque, P. 1991, Third Reference Catalog of Bright Galaxies (Austin: Univ. Texas Press)
de Vaucouleurs, G., de Vaucouleurs, A., & Pence, W. 1974, ApJ, 194, L119
De Young, D., & Heckman, T. M. 1994, ApJ, 431, 598
Driver, S. P., Windhorst, R. A. W., & Griffiths, R. E. 1995a, ApJ, 453. 48
Driver, S. P., Windhorst, R. A., Ostrander, E. J., Keel, W. C., Griffiths, R. E., & Ratnatunga, K. U. 1995b, ApJ, 449, L23
Ellis, T., et al. 1993, Proc. SPIE, 1765, 94
Fabbiano, G., Kim, D.-W., & Trinchieri, G. 1992, ApJS, 80, 531
Ferguson, H. C., & Binggeli, B. 1994, Astron. Astrophys. Rev., 6, 67
Gallagher, J. S., III, & Wyse, R. F. G. 1994, PASP, 106, 1225
George, I. M., Arnaud, K. A., Pence, B., & Ruamsuwan, L. 1992, Legacy, 2, 51
Glazebrook, K., Ellis, R. S., Santiago, B., & Griffiths, R. E. 1995, MNRAS, 275, L19
Green, P. J., Anderson, S. F., & Ward, M. J. 1992, MNRAS, 254, 30
Griffiths, R. E., Della Ceca, R., Georgantopoulus, I., Boyle, B. J., Stewart, G. C., Shanks, T., & Fruscione, A. 1996, MNRAS, 281, 71
Griffiths, R. E., & Padovani, P. 1990, ApJ, 360, 483
Heckman, T. M., Dahlem, M., Lehnert, M. D., Fabbiano, G., Gilmore, D., & Waller, W. H. 1995, ApJ, 448, 98 (H95)
Hensler, G., Theis, C., & Burkert, A. 1993, in The Feedback of Chemical Evolution on the Stellar Content of Galaxies, ed. D. Alloin & G. Stasinska (Paris: l'Observatoire de Paris), 229
Hodge, P. 1974, ApJ, 191, L21
Hunter, D., & Gallagher, J. S., III. 1989, Science, 243, 1557
Hunter, D. A., Hawley, W. N., & Gallagher, J. S., III. 1993, AJ, 106, 1797
Ingham, J. 1994, XSELECT User's Guide (Greenbelt: NASA/GSFC)
Israel, F. P. 1988, A&A, 194, 24
Israel, F. P., & de Bruyn, A. G. 1988, A&A, 198, 109
Israel, F. P., & van Driel, W. 1990, A&A, 236, 323
Lynden-Bell, D. 1992, in Elements and the Cosmos, ed. M. Edmunds & R. Terlevich (Cambridge: Cambridge Univ. Press), 270
Marlowe, A. T., Heckman, T. M., Wyse, R. F. G., & Schommer, R. 1995, ApJ, 438, 563
Martin, C. L. 1996, ApJ, 465, 680
Meurer, G. R., Freeman, K. C., Dopita, M. A., & Cacciari, C. 1992, AJ, 103, 60
Nandra, K. 1995, Calibration memo on NGC 5548, NASA/GSFC
O'Connell, R. W., Gallagher, J. S., & Hunter, D. A. 1994, ApJ, 433, 65
Petre, R. 1993, in The Nearest Active Galaxies, ed. J. Beckman, L. Colina, & H. Netzer (Madrid: CSIC), 117
Pfeffermann, E., et al. 1987, Proc. SPIE, 733, 519
Reakes, M. 1980, MNRAS, 192, 297
Rosati, P. 1995, PhD thesis, Univ. of Rome
Saracco, P., Chincarini, G., & Iovino, A. 1996, MNRAS, submitted
Tanaka, Y., Inoue, H., & Holt, S. S. 1994, PASJ, 46, L37
Tomita, A., Ohta, K., & Saito, M. 1994, PASJ, 46, 335
Treyer, M. A., Mouchet, M., Blanchard, A., & Silk, J. 1992, A&A, 264, 11
Waller, W. 1991, ApJ, 370, 144
Wang, Q. D., Walterbos, R. A. M., Steakley, M. F., Norman, C. A., & Braun, R. 1995, ApJ, 439, 176
Yoshii, Y., & Arimoto, N. 1987, A&A, 188, 13